Density Functional Calculations of Structures, Vibrational Frequencies, and Normal Modes of *trans*- and *cis*-Azobenzene

Nandita Biswas and Siva Umapathy*

Department of Inorganic and Physical Chemistry, Indian Institute of Science, Bangalore-560012, India

Received: January 24, 1997; In Final Form: May 7, 1997[⊗]

The vibrational structures of *trans*- (TAB) and *cis*-azobenzene (CAB) are of interest due to their importance in optoelectronic applications as well as due to the unique isomerization mechanism involving the inversion process (at the nitrogen site). In this paper, we report the equilibrium structures, harmonic frequencies, and mode assignments for TAB and CAB and their isotopic analogues, using restricted Hartree−Fock (RHF), hybrid Hartree−Fock/density functional (HF/DF), and pure density functional theoretical (DFT) methods utilizing the 6-31G* basis set. The results of the optimized molecular structure obtained on the basis of RHF and all the DFT calculations are presented and then critically compared with the experimental electron diffraction results. It is observed that best structural parameters are predicted by the hybrid HF/DF method, *viz.* B3LYP and B3P86 followed by the pure DFT method BP86. In the case of harmonic vibrational frequencies (unscaled) and the normal modes, it is found that the BP86/6-31G* is the most accurate. The data obtained here has been used to reassign (in contrast to the previously reported MP2 results) some of the vibrational frequencies, particularly, for the main N═N and C−N vibrations of TAB. On the basis of BP86/6-31G* force field, the infrared intensities for both TAB and CAB and their isotopomers have also been calculated. Moreover, the main differences in the vibrational spectra of the two isomers of azobenzene have been discussed from normal mode analysis.

Introduction

The structure of azo dyes have attracted considerable attention in recent times due to their wide applicability in light-induced photoisomerization,[1] and, therefore, their potential use for reversible optical data storage.[2−7] These applications typically utilize the fast isomerization phenomenon as a molecular switch.[2a−g] Recently, numerous publications have appeared on the azobenzene isomerization processes.[1−14] Since the azo group consists of sp^2-hybridized nitrogen atoms, the isomerization involves two possible mechanisms,[15] one involving rotation about the central N═N bond and the other involving in-plane inversion about one of the N atoms *via* a linear transition state. The inversion route is unique to azobenzene, unlike the rotation mechanism which has been well studied in isoelectronic systems such as *cis*- and *trans*-stilbene.[16−22] The mechanism of isomerization, in general, of aromatic azo compounds has not been well understood[1,9] and has drawn the interest of various research groups at present.[1−14] Regarding the structure of *trans*-azobenzene (TAB) in its ground electronic state, it is not yet established whether the molecule is planar (C_{2h}) or slightly distorted from planarity (C_i).[23−25] The crystal structure[26] suggests that TAB is planar whereas gas-electron diffraction measurements[27] show that the phenyl rings are rotated by 30° with respect to the N═N−C plane. The absence of unpolarized Raman bands for TAB and its isotopic analogues led to the conclusion that it has C_i molecular symmetry in solution.[25] X-ray diffraction studies for *cis*-azobenzene (CAB)[28] suggest a nonplanar structure consisting of a 2-fold axis of symmetry with the phenyl rings rotated 53.3° about the N═N−C plane.

To elucidate the structural properties of the azo compounds, various spectroscopic and photochemical methods including UV−vis absorption,[29−33] femtosecond time-resolved absorption,[34] infrared (IR),[35,36] Raman,[14,37−48] and NMR[49] have been extensively used. In particular, from resonance Raman (RR) intensities, ultrafast dynamical information of the isomerization process can also be obtained.[14] Accurate normal mode analysis for TAB and CAB is essential to understand the mode-dependent structural distortions involved during the isomerization phenomenon. However, the analysis of vibrational data[37−48,50,51] for TAB has been qualitative both in terms of assignments as well as the description of normal modes. In a recent report, Armstrong *et al.*[51] have presented the normal mode analysis for TAB with the optimized geometry resulting in two imaginary vibrational frequencies (indicating a transition state structure) and some of the vibrational assignments not matching the experimental data.

Density functional theory (DFT) is being widely used for computation of molecular structure and vibrational frequencies.[52−68] In particular, for polyatomic molecules (typically normal modes exceeding 50) the DFT methods lead to the prediction of more accurate molecular structure and vibrational frequencies than the conventional *ab initio* restricted Hartree−Fock (RHF) and MP2 calculations. Computed frequencies using MP2 are relatively close to experimental results (compared to those of RHF) due to the inclusion of electron correlation.[69] Another widely used method for computing the vibrational frequencies of polyatomic molecules is the scaled quantum mechanical (SQM) force field methodology of Pulay's group.[70] For systems, such as, *trans*- and *cis*-stilbene, which are isoelectronic to azobenzene, complete vibrational analysis has been carried out by Arenas *et al.*[71] using this SQM approach. Since stilbene consists of two benzene rings joined by an ethylene moiety, the force constants for benzene and ethylene are first computed using the RHF method, and then using various empirical scale factors, these force constants are refined and subsequently transferred to the parent molecule, stilbene. The scale factors generally remove the anomalies present in the

* Author to whom correspondence should be addressed. Email: suma@hamsadvani.serc.iisc.ernet.in. Fax: 91-80-3316552.

⊗ Abstract published in *Advance ACS Abstracts,* June 15, 1997.

S1089-5639(97)00312-5 CCC: $14.00

calculated frequencies due to neglect of electron correlation effects, basis set deficiencies, anharmonicity effects, *etc*. As a result, the SQM method reduces the standard deviation of the calculated frequencies to within 10 cm^{-1} of the experimental values.[72,73] The only disadvantage of the SQM force field method is that it is very tedious, since separate scaling factors have to be used for individual internal coordinates (stretching, bending, *etc*.). Interestingly, DFT calculations have also been successfully used only for the computation of vibrational frequencies for polyatomic systems such as fluorene[58] (consisting of 63 normal modes), carbazole[59] (60 normal modes), 2,3-dimethoxy-1,4-benzoquinone[60] (54 normal modes), *etc*., but accurate mode descriptions in terms of potential energy distributions (PEDs) for each mode have not been addressed.

The main objectives for carrying out the present investigation are as follows: (a) to obtain an accurate force field, which is necessary to get vibrational mode dependent isomerization dynamical information of TAB from RR intensities,[14,74] (b) to obtain PEDs and exact normal mode descriptions, which are not available in the literature for CAB and TAB but are necessary for the accurate assignment of the vibrational spectra of azo dyes,[37−48,50,51] (c) to clarify the deviations in the calculated vibrational frequencies for various isotopes of TAB, with respect to the experimental data, for the main vibrations such as N═N and C−N in comparison to results obtained using the MP2 method,[51] (d) to evaluate the use of DFT methods in predicting accurate normal mode descriptions of polyatomic molecules in addition to vibrational frequencies, and (e) to compare the calculated IR intensities with those obtained from experiments.[35] A comparative study of RHF, hybrid Hartree−Fock/density functional (HF/DF), and DFT methods have been carried out for TAB and CAB (including their isotopic analogues), and the results are critically compared with the available experimental frequencies[25,35] and the previously published MP2 calculations.[51] We have also examined the differences in the vibrational spectra of both isomers of azobenzene in relation to their respective molecular structures.

Computational Details

The *ab initio* RHF as well as all DFT calculations presented here have been carried out using the Gaussian 94 set of programs[75] on an IBM-RS6000 computer system. The molecular geometries of TAB and CAB are optimized using RHF and five DFT methods, with the 3-21G, 6-31G and 6-31G* basis sets. The five density functionals employed in the present study are (1) Becke's three-parameter hybrid method[76,77] using the LYP correlation functional[78] (B3LYP), (2) Becke's three-parameter hybrid method[76,77] using the Perdew 86 expression[79] (B3P86), (3) SVWN, which takes into account a local spin density exchange by Slater[80] combined with the correlation function of Vosko, Wilk, and Nusair[81], (4) BLYP which includes Becke's 1988 exchange functional,[77] *i.e*. the Slater exchange along with corrections involving the gradient of the density combined with the correlation function of Lee-Yang and Parr,[78] and (5) Becke's 1988 exchange functional[77] combined with the gradient-corrected correlation function of Perdew[79] (BP86).

Berny's optimization algorithm[82] was used to carry out the complete geometry optimization for both isomers of azobenzene, and this resulted in C_i symmetry for TAB and C_2 symmetry for CAB. The normal modes and vibrational frequencies were then evaluated at the computed equilibrium geometries by analytic evaluation of the second derivatives of energy. PEDs of normal modes were calculated from the quantum mechanically derived Cartesian force constant matrix using MOLVIB.[83] The root mean square (RMS) deviation of the computed frequencies relative to the experimental values for various density functionals and the MP2[51] method were also calculated.[57,61]

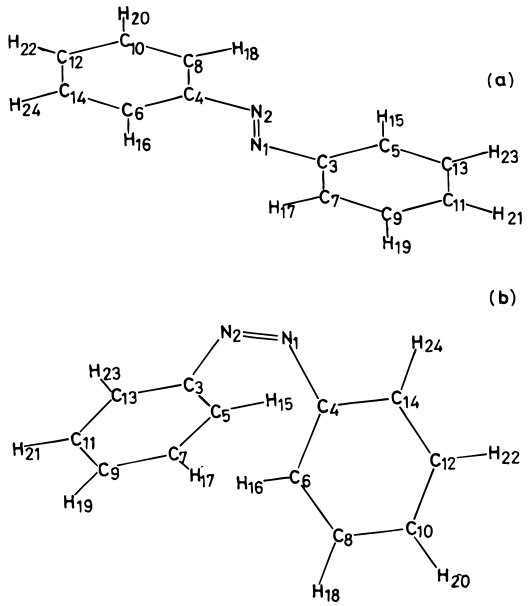

Figure 1. Optimized geometry and atom numbering of (a) *trans*-azobenzene and (b) *cis*-azobenzene.

Results and Discussion

***trans*-Azobenzene (TAB). Geometrical Structure.** The structure of TAB has been a subject of controversy for several years. The X-ray diffraction (XRD)[26] result suggests a planar structure. On the other hand, gas-phase electron diffraction (ED)[27] studies suggest a nonplanar structure. ED results show that the phenyl ring is twisted by 30° (C_i symmetry) around the N═N−C plane. This distorted structure is also found to be present in solution and has been supported by the Raman measurements on TAB and its isotopomers.[25] All our DFT as well as RHF calculations adopt C_i geometry for TAB. The numbering of the atoms in TAB is depicted in Figure 1a. The optimized parameters, *i.e*. the bond lengths and bond angles, of TAB are computed by RHF, B3LYP, B3P86, SVWN, BLYP, and BP86 using three different (3-21G, 6-31G, and 6-31G*) basis sets. For the sake of convenience, only the optimized parameters obtained from the qualitatively superior split valence and polarized 6-31G* basis set corresponding to each functional along with the experimental parameters are presented in Table 1. The complete chart containing the optimized parameters obtained from RHF, B3LYP, B3P86, SVWN, BLYP, and BP86 using the basis sets 3-21G, 6-31G, and 6-31G* is available as Supporting Information (Tables ISa−ISc).

The optimized bond lengths obtained from the DFT methods are generally overestimated with respect to the XRD values but are comparable to the ED results. Hence, the calculated bond distances and bond angles obtained from all density functionals and the conventionally used *ab initio* RHF method have been compared with the available ED data. It is interesting to note that RHF/6-31G* underestimates the N═N bond distance by 0.049 Å, but the optimized C−N, C−C, and C−H bond lengths deviate only by 0.007 Å, 0.010 Å, and 0.014 Å, respectively. The C−N═N and C−C−N bond angles calculated by RHF method are overestimated by 1.2° and 1.4° relative to the ED values. Since the ED values for C−C−C and C−C−H bond angles are not available, a comparative study of the calculated bond angles for the same angles obtained from RHF and the density functionals is not possible. For the three-parameter hybrid HF/DF method B3LYP/6-31G*, the N═N bond length varies relative to the ED value by 0.008 Å. Similarly, the

TABLE 1: Optimized Geometrical Parameters of *trans*-Azobenzene in its Ground State

							expt	
	RHF/6-31G*	B3LYP/6-31G*	B3P86/6-31G*	SVWN/6-31G*	BLYP/6-31G*	BP86/6-31G*	X-ray[a]	ED[b]
				Bond Lengths (Å)				
$N^2{=}N^1$	1.219	1.260	1.257	1.263	1.282	1.279	1.247	1.268
$C^3{-}N^1$	1.420	1.418	1.411	1.396	1.426	1.421	1.428	1.427
$C^5{-}C^3$	1.392	1.405	1.402	1.399	1.418	1.415	1.389	1.396
$C^7{-}C^3$	1.385	1.401	1.397	1.395	1.413	1.411	1.387	1.396
$C^9{-}C^7$	1.386	1.393	1.390	1.387	1.403	1.401	1.384	1.396
$C^{11}{-}C^9$	1.383	1.395	1.392	1.390	1.406	1.404	1.382	1.396
$C^{13}{-}C^{11}$	1.390	1.401	1.397	1.396	1.411	1.409	1.391	1.396
$C^{13}{-}C^5$	1.380	1.389	1.386	1.382	1.398	1.397	1.384	1.396
$H^{15}{-}C^5$	1.072	1.084	1.084	1.095	1.091	1.093		1.088
$H^{17}{-}C^7$	1.074	1.085	1.085	1.095	1.093	1.095		1.088
$H^{19}{-}C^9$	1.075	1.086	1.086	1.095	1.093	1.095		1.088
$H^{21}{-}C^{11}$	1.075	1.086	1.086	1.095	1.094	1.095		1.088
$H^{23}{-}C^{13}$	1.075	1.086	1.086	1.096	1.094	1.096		1.088
				Bond Angles (deg)				
$C^3{-}N^1{=}N^2$	115.7	114.7	114.5	114.3	114.4	114.1	114.1	114.5
$C^5{-}C^3{-}N^1$	124.4	124.7	124.6	124.0	125.1	124.9	123.7	123.0
$C^7{-}C^3{-}N^1$	115.4	115.3	115.3	115.7	115.1	115.1	115.6	
$C^3{-}C^5{-}C^{13}$	119.4	119.5	119.5	119.5	119.6	119.6	119.1	
$C^3{-}C^7{-}C^9$	120.2	120.2	120.1	120.0	120.2	120.2	119.6	
$C^5{-}C^{13}{-}C^{11}$	120.4	120.4	120.4	120.3	120.4	120.4	120.5	
$C^5{-}C^3{-}C^7$	120.0	119.8	119.9	120.1	119.7	119.8	120.7	
$C^{13}{-}C^{11}{-}C^9$	119.9	120.0	120.0	120.2	120.0	120.0	119.7	
$C^{11}{-}C^9{-}C^7$	119.8	119.8	119.7	119.7	119.8	119.8	120.3	
$H^{15}{-}C^5{-}C^3$	119.6	118.8	118.6	117.5	118.6	118.5		
$H^{15}{-}C^5{-}C^{13}$	120.8	121.5	121.7	122.9	121.6	121.8		
$H^{23}{-}C^{13}{-}C^5$	119.6	119.7	119.7	119.9	119.7	119.7		
$H^{23}{-}C^{13}{-}C^{11}$	119.8	119.8	119.8	119.7	119.7	119.7		
$H^{21}{-}C^{11}{-}C^{13}$	119.9	119.9	119.9	119.8	119.9	119.9		
$H^{21}{-}C^{11}{-}C^9$	120.1	120.0	120.0	119.9	120.0	120.0		
$H^{19}{-}C^9{-}C^{11}$	120.2	120.1	120.1	120.1	120.1	120.1		
$H^{19}{-}C^9{-}C^7$	119.9	119.9	120.0	120.0	119.9	119.9		
$H^{17}{-}C^7{-}C^9$	121.0	121.5	121.6	122.3	121.6	121.7		
$H^{17}{-}C^7{-}C^3$	118.7	118.2	118.1	117.6	118.0	118.0		

[a] Reference 26. [b] Reference 27.

average C−N, C−C, and C−H bond lengths differ from the ED data by 0.009 Å, 0.005 Å, and 0.003 Å, respectively. The C−N═N and C−C−N bond angles deviate by 0.2° and 1.7° from the experimental value. Similarly, the three-parameter hybrid HF/DF method B3P86/6-31G* predicts the N═N, C−N, C−C, and C−H bond lengths quite accurately, and the calculated deviations for the same lengths are 0.011 Å, 0.016 Å, 0.005 Å, and 0.003 Å, respectively, and those calculated for C−N═N and C−C−N bond angles are 0.0° and 1.6°. Hence, B3P86 method predicts bond distances and bond angles comparable to B3LYP, but the calculated bond lengths deviate considerably for N═N and C−N. The calculated bond distances as well as bond angles using the local DFT method (SVWN/6-31G*) is relatively good with the exception of the C−N bond length which deviates by 0.031 Å from the experimental bond length. The nonlocal DFT methods, BLYP/6-31G* and BP86/6-31G*, predict accurate bond distances which are close to the experimental values; however, the calculated C−C−N bond angle deviates considerably for BLYP (2.1°) as compared to BP86 (1.9°). Overall, we find that the optimized bond lengths and bond angles calculated from B3LYP/6-31G* gives the best structural parameters followed by the B3P86/6-31G* and BP86/6-31G* methods.

Fundamental Frequencies of TAB. The 66 fundamentals of TAB span the representation $\Gamma = 33A_g + 33A_u$ vibrations. Due to the presence of the inversion center in TAB, 33 A_g modes are Raman active whereas 33 A_u modes are IR active. The 33 Raman active modes of TAB consist of 23 in-plane (ip) and 10 out-of-plane (oop) vibrations. Similarly, 33 IR active modes consist of 22 ip and 11 oop vibrations. The calculated frequencies and normal mode descriptions of the 66 normal vibrations of TAB from the three DFT methods, B3LYP, B3P86, and BP86, with 6-31G* (those which yield the best structural parameters) have been compared with the experimental Raman[25] and IR spectra.[35] A comparative study of these (unscaled) computed frequencies along with the previously published MP2/6-31G$^\alpha$ data[51] and the experimental frequencies[25,35] are given in Table 2. (All the results using other functional forms and basis sets are available as Supporting Information, Tables IISa−IISf). It is seen that the hybrid HF/DF methods, *viz.* B3LYP/6-31G* and B3P86/6-31G*, show a general trend of overestimating the calculated frequencies, whereas the computed frequencies from the nonlocal DFT method, BP86/6-31G*, are generally underestimated, with the exception of only a few vibrational modes. The RMS deviations have also been calculated with and without the inclusion of C−H stretch for the unscaled frequencies obtained from the above mentioned methods. The RMS deviations for B3LYP/6-31G*, B3P86/6-31G*, BP86/6-31G*, and MP2/6-31G$^\alpha$ [51] with the C−H stretch are 72, 79, 29, and 81 cm^{-1}, respectively. Similarly, the RMS deviations without the inclusion of the C−H stretch for B3LYP/6-31G*, B3P86/6-31G*, BP86/6-31G*, and MP2/6-31G$^\alpha$ [51] are 34, 36, 11, and 58 cm^{-1}, respectively. It is observed that inclusion of the C−H stretch leads to greater RMS deviation. This is expected because all the DFT methods are known to overestimate the C−H stretching frequencies.[61,62] Maximum deviation is observed for the computed frequencies from the MP2 results followed by B3P86, B3LYP, and BP86. Thus, it is apparent that usually the DFT methods give better results than the MP2 calculation, and minimum deviation is observed for the BP86/6-31G* method. Hence, the PEDs have been calculated using the BP86/6-31G* force field and are presented in Table 2 for the ip and oop A_g and A_u modes. It is observed that though TAB is nonplanar, having C_i symmetry (optimized

TABLE 2: Symmetries, Calculated Frequencies (in cm^{-1}), and PEDs for the A_g and A_u Normal Vibrations of *trans*-Azobenzene Using a Variety of Quantum Mechanical Methods[a]

A_g Normal Vibrations (In-Plane Modes $\nu_1-\nu_{23}$, Out-of-Plane Modes $\nu_{24}-\nu_{33}$)

mode	character	B3LYP 6-31G*	B3P86 6-31G*	BP86 6-31G*	MP2[b] 6-31G$^\alpha$	expt[c]	PED (%)[d]
ν_1	υ(C−H)	3233	3244	3143	3221	3085	99 υ(C−H)
ν_2	υ(C−H)	3216	3231	3131	3210	3073	98 υ(C−H)
ν_3	υ(C−H)	3205	3221	3120	3197	3066	98 υ(C−H)
ν_4	υ(C−H)	3194	3210	3109	3187	3060	97 υ(C−H)
ν_5	υ(C−H)	3184	3200	3099	3178	3044	98 υ(C−H)
ν_6	υ(C−C)	1660	1676	1605	1622		74 υ(C−C), 16 δ(C−C)
ν_7	υ(C−C)	1645	1661	1589	1614	1595	62 υ(C−C), 25 δ(C−C)
ν_8	υ(C−C)	1521	1579	1486	1519	1493	38 υ(C−C), 27 υ(N═N), 17 δ(C−N), 11 δ(C−H)
ν_9	υ(C−C)	1492	1525	1465	1504	1473	48 υ(C−C), 21 δ(C−N), 13 δ(C−H), 10 δ(C−C)
ν_{10}	υ(N═N)	1560	1500	1420	1450	1443	54 υ(N═N), 25 υ(C−C)
ν_{11}	υ(C−C)	1370	1398	1367	1395	1379	95 υ(C−C)
ν_{12}	δ(C−H)	1350	1346	1300	1368	1315	39 δ(C−H), 24 δ(C−N), 17 υ(C−C)
ν_{13}	υ(C−C)	1216	1226	1181	1235	1184	35 υ(C−C), 31 υ(C−N), 15 δ(C−C), 13 δ(C−H)
ν_{14}	δ(C−H)	1191	1190	1157	1226	1158	53 δ(C−H), 45 υ(C−C)
ν_{15}	υ(C−N)	1172	1178	1131	1195	1146	38 υ(C−N), 24 υ(C−C), 21 δ(C−C)
ν_{16}	υ(C−C)	1105	1106	1071	1110	1071	63 υ(C−C), 16 δ(C−C), 10 δ(C−N), 10 δ(C−H)
ν_{17}	υ(C−C)	1048	1054	1018	1047	1023	72 υ(C−C), 22 δ(C−C)
ν_{18}	δ(C−C)	1018	1019	986	1024	1003	78 δ(C−C), 17 υ(C−C)
ν_{19}	δ(C−C)	940	946	912	933	913	50 δ(C−C), 29 υ(C−C), 10 δ(N═N)
ν_{20}	δ(C−C)	684	683	662	691	670	79 δ(C−C), 11 δ(C−N)
ν_{21}	δ(C−C)	627	624	605	634	614	95 δ(C−C)
ν_{22}	δ(C−N)	307	308	298	307		76 δ(C−N), 10 δ(C−C)
ν_{23}	δ(C−N)	224	224	216	226	219	69 δ(C−N), 22 δ(C−C)
ν_{24}	γ(C−H)	1006	1007	962	857	968	52 γ(C−H), 47 τ(C−C)
ν_{25}	γ(C−H)	985	987	941	851	938	50 γ(C−H), 50 τ(C−C)
ν_{26}	γ(C−H)	948	948	907	825		55 γ(C−H), 43 τ(C−C)
ν_{27}	γ(C−H)	865	864	830	778	836	100 γ(C−H)
ν_{28}	τ(C−C)	781	780	752	702	755	63 τ(C−C), 34 γ(C−H)
ν_{29}	τ(C−C)	699	699	673	444		86 τ(C−C), 13 γ(C−H)
ν_{30}	τ(C−C)	492	490	471	400		70 τ(C−C), 23 γ(C−H)
ν_{31}	τ(C−C)	423	421	405	381	403	95 τ(C−C)
ν_{32}	τ(C−C)	260	260	245	213	251	72 τ(C−C), 17 τ(C−N)
ν_{33}	τ(C−C)	109	108	105	−85		68 τ(C−C), 27 τ(C−N)

A_u Normal Vibrations (In-Plane Modes $\nu_{45}-\nu_{66}$, Out-of-Plane Modes $\nu_{34}-\nu_{44}$)

		B3LYP		B3P86		BP86		MP2[b]		
mode	character	6-31G*	I[e]	6-31G*	I	6-31G*	I	6-31G$^\alpha$	expt[f]	PED (%)[d]
ν_{45}	υ(C−H)	3233	9.0	3244	9.7	3143	13.7	3221	3081	99 υ(C−H)
ν_{46}	υ(C−H)	3216	36.3	3231	36.8	3131	49.9	3210	3065	98 υ(C−H)
ν_{47}	υ(C−H)	3205	64.0	3221	47.2	3120	59.8	3197	3053	98 υ(C−H)
ν_{48}	υ(C−H)	3194	28.6	3210	22.2	3109	27.3	3187	3036	97 υ(C−H)
ν_{49}	υ(C−H)	3183	2.6	3199	3.0	3099	5.6	3178	3020	98 υ(C−H)
ν_{50}	υ(C−C)	1656	3.6	1673	4.0	1603	6.0	1623		73 υ(C−C), 16 δ(C−C)
ν_{51}	υ(C−C)	1639	4.7	1655	5.0	1585	3.9	1609	1585 m	65 υ(C−C), 26 δ(C−C)
ν_{52}	υ(C−C)	1534	10.0	1538	10.7	1481	8.1	1524	1486 s	64 υ(C−C), 26 δ(C−H)
ν_{53}	υ(C−C)	1500	11.6	1503	13.8	1452	11.9	1494	1456 s	55 υ(C−C), 17 δ(C−N), 15 δ(C−C), 13 δ(C−H)
ν_{54}	υ(C−C)	1368	8.1	1395	8.4	1364	6.6	1392	1399 w	95 υ(C−C)
ν_{55}	δ(C−N)	1343	2.4	1339	1.6	1295	2.0	1363	1300 m	38 δ(C−N), 34 δ(C−H), 23 υ(C−C)
ν_{56}	υ(C−N)	1263	23.0	1280	29.1	1228	22.6	1270	1223 m	42 υ(C−N), 25 δ(C−C), 23 υ(C−C)
ν_{57}	δ(C−H)	1191	0.1	1190	0.2	1157	0.3	1226	1160 w	52 δ(C−H), 46 υ(C−C)
ν_{58}	υ(C−C)	1185	34.9	1183	31.3	1145	36.9	1211	1152 m	34 υ(C−C), 21 δ(C−C), 21 δ(C−H), 17 υ(C−N)
ν_{59}	υ(C−C)	1108	10.9	1110	13.8	1075	13.6	1114	1072 m	61 υ(C−C), 16 δ(C−C), 12 δ(C−N), 11 δ(C−H)
ν_{60}	υ(C−C)	1048	19.8	1053	11.3	1017	10.3	1047	1020 m	75 υ(C−C), 18 δ(C−C)
ν_{61}	δ(C−C)	1018	3.3	1019	3.8	985	4.0	1025	1000 w	79 δ(C−C), 15 υ(C−C)
ν_{62}	δ(C−C)	840	0.6	846	0.7	816	0.8	834	813 w	63 δ(C−C), 24 υ(C−C), 12 υ(C−N)
ν_{63}	δ(C−C)	633	0.6	631	0.7	611	0.7	640	615 w	90 δ(C−C)
ν_{64}	δ(C−C)	547	6.6	545	6.0	528	6.9	555	545 s	62 δ(C−C), 30 δ(C−N)
ν_{65}	δ(C−N)	530	25.4	532	25.7	515	23.7	524	521 s	56 δ(C−N), 34 δ(C−C)
ν_{66}	δ(C−N)	86	1.8	86	1.8	83	1.8	86		76 δ(C−N), 11 δ(N═N)
ν_{34}	γ(C−H)	1007	1.0	1008	1.1	962	1.1	860	985 w	51 γ(C−H), 48 τ(C−C)
ν_{35}	γ(C−H)	985	0.0	987	0.0	941	0.1	851		50 γ(C−H), 50 τ(C−C)
ν_{36}	γ(C−H)	953	7.8	953	9.4	912	8.1	828	927 s	50 γ(C−H), 49 τ(C−C)
ν_{37}	γ(C−H)	864	0.0	863	0.0	829	0.0	775	850 w	100 γ(C−H)
ν_{38}	τ(C−C)	800	56.6	800	64.1	771	57.4	708	776 s	67 τ(C−C), 27 γ(C−H)
ν_{39}	τ(C−C)	706	55.7	705	67.7	679	60.3	542	689 s	79 τ(C−C), 19 γ(C−H)
ν_{40}	τ(C−C)	561	7.1	560	9.5	538	7.9	418	545 s	73 τ(C−C), 19 γ(C−H)
ν_{41}	τ(C−C)	420	0.0	418	0.0	401	0.0	387		95 τ(C−C)
ν_{42}	τ(C−C)	309	0.8	308	0.7	295	0.8	280		81 τ(C−C), 13 γ(C−H)
ν_{43}	τ(N═N)	64	1.2	64	1.4	61	1.4	59		57 τ(N═N), 27 τ(C−C), 13 γ(C−N)
ν_{44}	τ(C−N)	25	0.0	27	0.0	25	0.1	−20		52 τ(C−N), 36 τ(C−C)

[a] υ indicates stretch; δ, in-plane bend; γ, out-of-plane bend; and τ, torsion. [b] Reference 51. [c] Reference 25. [d] PEDs calculated from BP86/6-31G*. [e] I represents the infrared intensities in km/mol: m, medium; s, strong; and w, weak. [f] Reference 35.

TABLE 3: Calculated Frequencies (in cm^{-1}) for Isotopic Derivatives of *trans*-Azobenzene for the A_g and A_u Normal Vibrations Obtained from the BP86/6-31G* Calculation

A_g Normal Vibrations (In-Plane Modes $\nu_1-\nu_{23}$, Out-of-Plane Modes $\nu_{24}-\nu_{33}$)

		$(C_6H_5N)_2$		$(C_6H_5)_2N^{15}N$	$(C_6H_5{}^{15}N)_2$		$(C_6D_5N)_2$	
mode	character	expt[a]	calc	calc	expt[a]	calc	expt[a]	calc
ν_1	υ(C−H)	3085	3143	3143		3143		2325
ν_2	υ(C−H)	3073	3131	3131		3131		2319
ν_3	υ(C−H)	3066	3120	3120	3070	3120	2298	2307
ν_4	υ(C−H)	3060	3109	3109		3109		2295
ν_5	υ(C−H)	3044	3099	3099		3099		2283
ν_6	υ(C−C)		1605	1604		1603	1586	1573
ν_7	υ(C−C)	1595	1589	1588	1595	1588	1562	1558
ν_8	υ(C−C)	1493	1486	1480	1485	1478	1341	1343
ν_9	υ(C−C)	1473	1465	1464	1471	1462	1331	1335
ν_{10}	υ(N═N)	1443	1420	1404	1412	1386	1468	1444
ν_{11}	υ(C−C)	1379	1367	1367		1366	1353	1366
ν_{12}	δ(C−H)	1315	1300	1299	1312	1297	1042	1029
ν_{13}	υ(C−C)	1184	1181	1179	1181	1178	960	946
ν_{14}	δ(C−H)	1158	1157	1157	1157	1157	861	852
ν_{15}	υ(C−N)	1146	1131	1128	1141	1125	1134	1125
ν_{16}	υ(C−C)	1071	1071	1071	1070	1071	844	838
ν_{17}	υ(C−C)	1023	1018	1018	1022	1018	825	804
ν_{18}	δ(C−C)	1003	986	986	1002	986	790	789
ν_{19}	δ(C−C)	913	912	903	901	894	912	901
ν_{20}	δ(C−C)	670	662	661	667	659	632	631
ν_{21}	δ(C−C)	614	605	605	614	604	588	580
ν_{22}	δ(C−N)		298	298		298		280
ν_{23}	δ(C−N)	219	216	216		216		205
ν_{24}	γ(C−H)	968	962	962	967	962		799
ν_{25}	γ(C−H)	938	941	941		941		761
ν_{26}	γ(C−H)		907	907		907		746
ν_{27}	γ(C−H)	836	830	830	839	830	550	539
ν_{28}	τ(C−C)	755	752	752		752	654	646
ν_{29}	τ(C−C)		673	673		673		627
ν_{30}	τ(C−C)		471	471		471		412
ν_{31}	τ(C−C)	403	405	405		405	354	355
ν_{32}	τ(C−C)	251	245	243	248	241	242	235
ν_{35}	τ(C−C)		105	105		104		101

A_u Normal Vibrations (In-Plane Modes $\nu_{45}-\nu_{66}$, Out-of-Plane Modes $\nu_{34}-\nu_{44}$)

		$(C_6H_5N)_2$			$(C_6H_5)_2N^{15}N$			$(C_6H_5{}^{15}N)_2$		$(C_6D_5N)_2$	
mode	character	expt[b]	calc	I[c]	expt[b]	calc	I	calc	I	calc	I
ν_{45}	υ(C−H)	3081	3143	13.7		3143	13.6	3143	13.7	2325	22.0
ν_{46}	υ(C−H)	3065	3131	49.9		3131	49.9	3131	49.9	2319	31.8
ν_{47}	υ(C−H)	3053	3120	59.8		3120	59.8	3120	59.8	2307	23.3
ν_{48}	υ(C−H)	3036	3109	27.3		3109	27.3	3109	27.3	2295	11.9
ν_{49}	υ(C−H)	3020	3099	5.6		3099	5.6	3099	5.6	2283	2.3
ν_{50}	υ(C−C)		1603	6.0		1603	5.8	1603	6.0	1570	9.2
ν_{51}	υ(C−C)	1585 m	1585	3.9	1585	1585	3.9	1585	3.9	1550	3.2
ν_{52}	υ(C−C)	1486 s	1481	8.1	1486	1481	5.7	1480	8.4	1334	4.8
ν_{53}	υ(C−C)	1456 s	1452	11.9	1456	1452	11.9	1452	12.0	1377	1.3
ν_{54}	υ(C−C)	1399 w	1364	6.6	1399	1364	6.6	1364	6.7	1356	8.4
ν_{55}	δ(C−N)	1300 m	1295	2.0	1300	1294	2.2	1294	2.2	1022	2.4
ν_{56}	υ(C−N)	1223 m	1228	22.6	1218	1224	20.8	1220	19.1	1172	21.5
ν_{57}	δ(C−H)	1160 w	1157	0.3	1160	1157	0.3	1157	0.3	946	0.7
ν_{58}	υ(C−C)	1152 m	1145	36.9	1152	1144	37.3	1144	38.5	866	0.2
ν_{59}	υ(C−C)	1072 m	1075	13.6	1072	1075	13.6	1075	13.5	839	2.8
ν_{60}	υ(C−C)	1020 m	1017	10.3	1020	1017	10.2	1017	10.2	818	23.4
ν_{61}	δ(C−C)	1000 w	985	4.0	1000	985	4.0	985	4.0	804	10.0
ν_{62}	δ(C−C)	813 w	816	0.8	810	812	0.8	808	0.8	752	5.2
ν_{63}	δ(C−C)	615 w	611	0.7	615	611	0.6	610	0.5	587	0.7
ν_{64}	δ(C−C)	545 s	528	6.9	544	525	8.0	522	8.9	513	8.2
ν_{65}	δ(C−N)	521 s	515	23.7	516	510	22.2	505	20.9	496	19.0
ν_{66}	δ(C−N)		83	1.8		83	1.7	82	1.7	78	1.5
ν_{34}	γ(C−H)	985 w	962	1.1	985	962	1.1	962	1.1	812	4.1
ν_{35}	γ(C−H)		941	0.1		941	0.1	941	0.1	762	1.0
ν_{36}	γ(C−H)	927 s	912	8.1	927	912	8.1	911	8.0	758	3.1
ν_{37}	γ(C−H)	850 w	829	0.0		829	0.0	829	0.0	541	32.9
ν_{38}	τ(C−C)	776 s	771	57.4	776	770	57.6	770	57.8	649	5.5
ν_{39}	τ(C−C)	689 s	679	60.3	689	679	60.2	679	60.1	645	0.0
ν_{40}	τ(C−C)	545 s	538	7.9	544	537	7.9	536	7.9	468	25.1
ν_{41}	τ(C−C)		401	0.0		401	0.0	401	0.0	351	0.0
ν_{42}	τ(C−C)		295	0.8		293	0.7	291	0.7	275	1.2
ν_{43}	τ(N═N)		61	1.4		61	1.3	61	1.3	58	1.2
ν_{44}	τ(C−N)		25	0.1		25	0.1	25	0.1	23	0.0

[a] Reference 25. [b] Reference 35. [c] I represents the infrared intensities in km/mol: m, medium; s, strong; w, weak.

structure is slightly distorted from planarity), the ip and oop vibrations do not mix significantly. The frequencies for the isotopic derivatives, $(C_6H_5)_2N^{15}N$, $(C_6H_5{}^{15}N)_2$, and $(C_6D_5N)_2$ have also been computed using BP86/6-31G* and are given in Table 3. The calculated IR intensities for TAB and its isotopes have been presented in Table 3 along with the experimental intensities.

In-Plane (ip) Vibrations of TAB. The ip modes of TAB, $\nu_1-\nu_5$ and $\nu_{45}-\nu_{49}$, are in the region of 3000 cm^{-1}. For these modes, there is a large shift (800 cm^{-1}) upon deuteration of the phenyl rings, indicating the fact that these modes correspond to the C−H stretch. The C−C stretching vibrations of TAB, ν_6, ν_7, ν_{50}, and ν_{51} undergo no change upon ^{15}N substitution as expected, but they do shift to low wavenumbers with D_{10} substitution as shown in Table 3. These modes are coupled to the ip C−C bend. The Raman active modes, ν_6 and ν_7, correspond to the symmetric C−C stretch, whereas IR active modes ν_{50} and ν_{51} correspond to the asymmetric C−C stretch. ν_{51} appears with medium intensity in the IR spectra which is in agreement with the calculated intensity (Table 3). ν_8, ν_9, ν_{52}, and ν_{53} correspond to the C−C stretch coupled with the C−N, C−H, and C−C ip bends with the exception of ν_8 which undergoes a shift of 8 cm^{-1} upon ^{15}N substitution of both N atoms, indicating the fact that ν_8 has some N═N stretching character too. ν_{52} and ν_{53} are intense in the IR spectra,[35] but the calculated intensity from BP86/6-31G* shows medium and strong intensity, respectively. Armstrong *et al.*[51] have reported that the Raman active mode ν_9 (C−C stretch) also has considerable contributions from N═N stretching character. But that is not observed in the present study, as shown in Table 2, instead, it consists of some ip C−N bending character. The absence of the contribution of the N═N stretch to ν_9 is supported by the experimental Raman data,[48] where it has been shown that as the excitation wavelength approaches the maxima of the $\pi \rightarrow \pi^*$ transition of TAB, only the ν_8 and ν_{10} modes are enhanced in intensity (**A** term enhancement), implying that these modes have a considerable amount of N═N stretch character. It is important to note here, that from a low-temperature absorption study of this transition, progressions of the N═N mode have also been observed.[33] The ν_{10} mode of TAB corresponds to the main azo N═N stretch. The calculated frequency of ν_{10} reduces by 16 cm^{-1} (1420 to 1404 cm^{-1}) when one of the N of the azo group is substituted by ^{15}N and by 34 cm^{-1} (1420 to 1386 cm^{-1}) when both the N atoms of the azo group are substituted by ^{15}N. Interestingly, the N═N stretch (ν_{10}) is also influenced by complete deuteration as evidenced by the shift of 24 cm^{-1} (1420 to 1444 cm^{-1}). These results are consistent with the experimental data,[25] where shifts of 31 cm^{-1} and 25 cm^{-1} are observed for $(C_6H_5{}^{15}N)_2$ and $(C_6D_5N)_2$, respectively. This is in contrast to the results of Armstrong *et al.*,[51] where the MP2/6-31G$^{\alpha}$ results showed only a slight increase (8 cm^{-1}) from 1450 to 1458 cm^{-1} for the main azo stretch (ν_{10}) upon ring deuteration which is three times less than the experimentally observed shift of 25 cm^{-1}. A comparative picture for the atomic displacements of the N═N stretching mode for (a) $(C_6H_5N)_2$, (b) $(C_6D_5N)_2$, and (c) $(C_6H_5{}^{15}N)_2$ is presented in Figure 2. As observed in the figure, the increase in frequency upon deuteration for the main azo stretch mode (ν_{10}) is due to the considerable contribution from the C−C stretch to the N═N stretch and also the reduced contribution from the C−D ip bend. From the PEDs (Table 2) it is also seen that the C−C stretch is coupled to the N═N stretch. However, the atomic displacements of the ν_{10} mode in $(C_6H_5{}^{15}N)_2$ are similar to that in $(C_6H_5N)_2$, indicating a reduction in frequency (1434 to 1399 cm^{-1}) due to the effective increase in reduced mass. All the modes except the main azo stretch

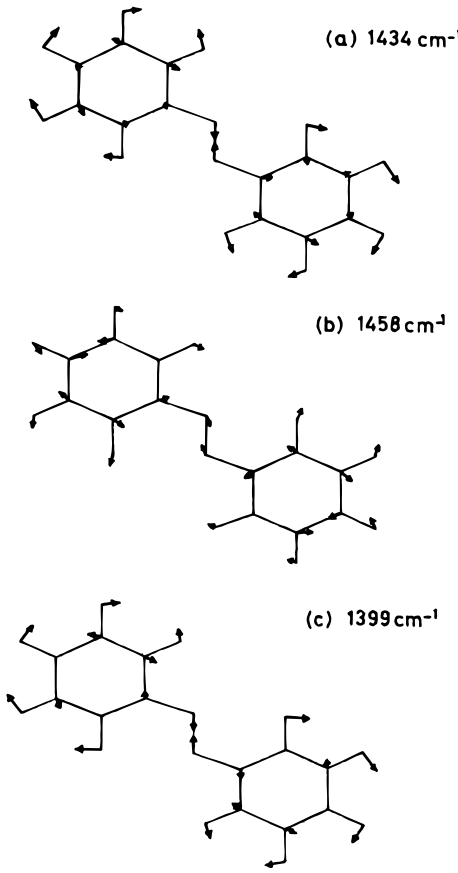

Figure 2. Calculated frequencies (in cm^{-1}) and atomic displacements of the N═N stretching mode of *trans*-azobenzene and its isotopic derivatives: (a) $(C_6H_5N)_2$, (b) $(C_6D_5N)_2$, and (c) $(C_6H_5{}^{15}N)_2$. The magnitude of displacement for the vibrating atoms is multiplied two times its true value.

undergo a decrease in frequency upon deuteration. Raman active mode, ν_{11}, and IR active mode, ν_{54}, are assigned purely to the C−C stretch. IR spectra[35] show a weak intensity for ν_{54}, but the calculation predicts medium intensity. The modes ν_{12}, ν_{14}, and ν_{57} mainly consist of the C−H ip bend and therefore show a large shift in frequency upon deuteration as shown in Table 3. The IR spectra of ν_{57} is observed to be weak from both calculation and experiment. The main Raman active mode for the symmetric C−N stretch calculated to be at 1131 cm^{-1} (ν_{15}) is quite close to that obtained from Raman measurements[25] at 1146 cm^{-1}. From the calculations, it is observed that this mode undergoes a shift of 6 cm^{-1} upon ^{15}N substitution of the azo group, where as the experimentally observed shift is 5 cm^{-1}. The asymmetric C−N stretch (ν_{56}) is at 1228 cm^{-1} and is predicted to be intense from calculation while the experimental IR band appears at 1223 cm^{-1} with medium intensity. Upon ^{15}N substitution of one of the N atoms of the azo group, the shift observed is 4 and 5 cm^{-1}, from calculation and experiment, respectively. The atomic displacements for the symmetric and asymmetric C−N stretching modes for (a) $(C_6H_5N)_2$, (b) $(C_6D_5N)_2$, and (c) $(C_6H_5{}^{15}N)_2$ are shown in Figures 3 and 4, respectively. Upon deuteration, the observed shifts (as seen from Table 3) are 6 cm^{-1} for ν_{15} and 57 cm^{-1} for ν_{56}, which is in contrast to the previously reported data of Armstrong *et al.*[51] where both modes ν_{15} and ν_{56} are shown to undergo a large shift in frequency upon deuteration due to the contribution from the C−D bend. Figures 3 and 4 clearly depict that the C−D bend does not have a significant contribution to the symmetric and asymmetric C−N stretch. The ν_{13} vibration mainly corresponds to the C−C stretch and is coupled to the C−N stretch, so it undergoes a shift of 3 cm^{-1} upon ^{15}N substitution of both N atoms in the azo group. The modes ν_{16}, ν_{17}, ν_{58-60}

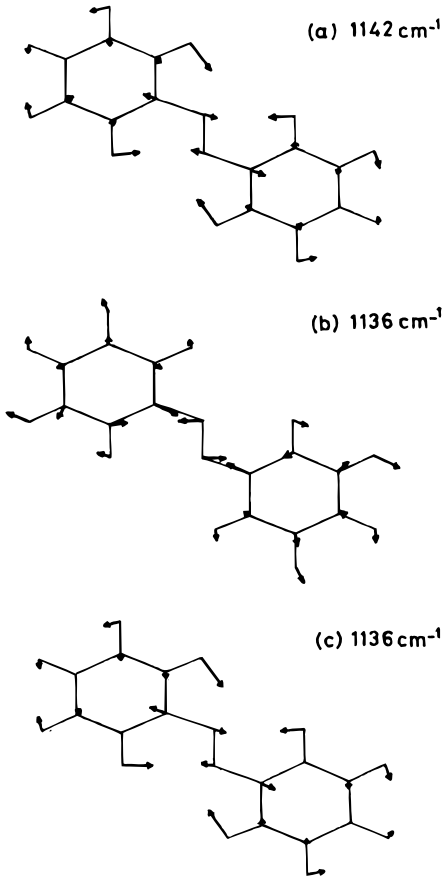

Figure 3. Calculated frequencies (in cm^{-1}) and atomic displacements of the symmetric C−N stretching mode of *trans*-azobenzene and its isotopic derivatives: (a) $(C_6H_5N)_2$, (b) $(C_6D_5N)_2$, and (c) $(C_6H_5{}^{15}N)_2$. The magnitude of displacement for the vibrating atoms is multiplied two times its true value.

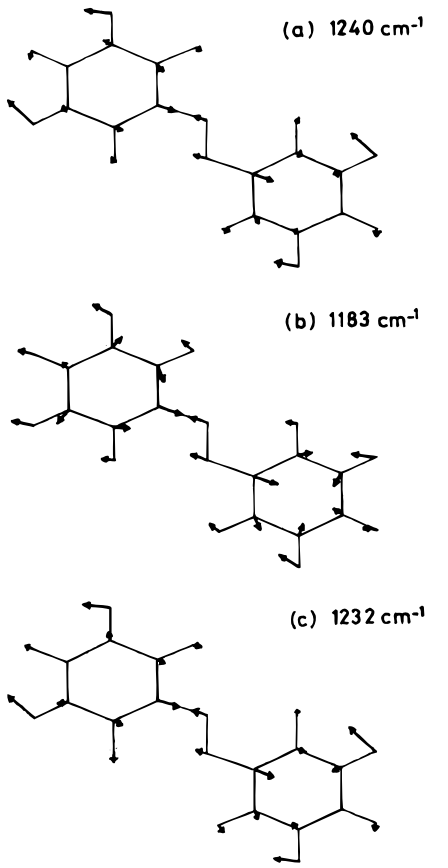

Figure 4. Calculated frequencies (in cm^{-1}) and atomic displacements of the asymmetric C−N stretching mode of *trans*-azobenzene and its isotopic derivatives: (a) $(C_6H_5N)_2$, (b) $(C_6D_5N)_2$, and (c) $(C_6H_5{}^{15}N)_2$. The magnitude of displacement for the vibrating atoms is multiplied two times its true value.

are mainly C−C stretches combined with the C−C ip bend. ν_{58-60} are shown to be of medium intensity from IR spectra, but BP86/6-31G* predicts these to be strong. ν_{21} and ν_{63} are purely C−C ip bends. ν_{63} is found to be weak in IR both from experiment and calculation. The modes, ν_{18-20}, ν_{61}, ν_{62}, and ν_{64} mainly correspond to the C−C ip bend. The vibrational mode ν_{19} shifts down by 18 cm^{-1} upon ^{15}N substitution confirming the contribution of the N═N ip bend. The mode ν_{62} also undergoes a down shift of 8 cm^{-1} due to the C−N stretching contribution. These two modes, ν_{19} and ν_{62}, also have contributions from the C−C stretch. The mode ν_{64} undergoes a shift of 6 cm^{-1} upon ^{15}N substitution, which is accounted for the C−N ip bend. ν_{61} and ν_{62} are of weak intensity from IR spectra, but calculation predicts medium and weak intensity for the same modes. Similarly, ν_{64} is expected to be strong from experiment, but calculation shows medium intensity. The low-frequency modes ν_{22}, ν_{23}, ν_{65}, and ν_{66} correspond to the C−N ip bend. The ν_{23} mode at 216 cm^{-1} was assigned to the N═N ip bend,[33] but from the calculated PEDs (Table 2), we reassign this vibration to the C−N ip bend. Both in the experiment and calculation, strong IR intensity is observed for ν_{65}. Thus, an overall one-to-one correspondence between the experimental and calculated frequencies (using BP86/6-31G*) has been observed for the ip vibrations.

Out-of-Plane (oop) Vibrations of TAB. TAB consists of 10 A_g Raman active and 11 A_u IR active oop vibrations. The vibrations ν_{24-26} and ν_{34-36} mainly correspond to the oop C−H bend and are coupled to the C−C torsion. These show a decrease of about 150 cm^{-1} upon deuteration. While calculation predicts medium IR intensities for ν_{34} and ν_{36}, experiment shows ν_{34} to be weak and ν_{36} to be strong. From the PEDs it is evident that ν_{27} and ν_{37} correspond to the oop C−H bend which undergoes a shift of about 300 cm^{-1} upon deuteration. ν_{37} appears to be very weak, both in experiment and calculation. The ν_{28-30}, ν_{38-40} and ν_{42} vibrations are assigned mainly to C−C torsion, coupled to the C−H oop bend. These modes almost remain unchanged in frequency by ^{15}N substitution; however, deuteration of phenyl rings results in a shift of about 50−100 cm^{-1}. ν_{38-40} appear as intense bands in IR spectra, which is in agreement with the calculation only for ν_{38} and ν_{39} whereas ν_{40} shows medium intensity. In the case of ν_{32} and ν_{33}, C−N torsion is coupled to the C−C torsion, as a result it undergoes a shift of 4 and 1 cm^{-1}, respectively upon complete isotopic substitution of the azo group by ^{15}N. The modes ν_{31} and ν_{41} are also assigned to C−C torsions. The frequencies for these modes reduce by 50 cm^{-1} upon deuteration as has been experimentally observed (49 cm^{-1}) from Raman measurements.[25] The vibration ν_{43} involves twisting about the N═N bond and is coupled to the C−C torsion and the C−N oop bend and ν_{44} involves torsion mainly about the C−N bond and also has contributions from the C−C torsion.

The data of Armstrong *et al.*[51] contains two imaginary frequencies for the two oop vibrations ν_{33} and ν_{44}, and the computed frequencies for these modes also deviate considerably from the experimental frequencies.[25,35] They attributed the negative value of the frequencies to the choice of the combined basis set 6-31G$^{\alpha}$ in which the basis set for the nitrogens were changed to 6-31+G(d) and the carbon and hydrogen atoms were treated with the 6-31G basis set. In contrast, our results indicate that BP86/6-31G* is quite accurate in reproducing the experimental frequencies along with a stable geometry.

Further, it has been reported[37] that the modes ν_{19} (912 cm^{-1}) and ν_{25} (941 cm^{-1}) are due to overtone and combination bands.

From the present study, it is observed that ν_{19} is a fundamental band assignable to the C−C ip bend coupled with the C−C stretch and the N═N ip bend. The vibration ν_{19} shifts by 18 cm^{-1} and 12 cm^{-1}, respectively, upon ^{15}N substitution in the calculated and experimental data. Similarly, ν_{25} is also a fundamental vibration assignable to the C−H oop bend, coupled to the C−C torsion which does not shift due to ^{15}N substitution, and shifts by 180 cm^{-1} upon deuteration. Overall, for TAB the computed frequencies for fundamental vibrations and the calculated values of isotopic shifts are very close to the experimental data.[25,35] Thus, we conclude that the DFT method BP86 with the 6-31G* basis set predicts accurate force fields for both the ip and oop modes of TAB, in contrast to the MP2 results.[51] Though the MP2 results are moderately close to the experimental frequencies for the ip modes but deviate to a large extent for the oop modes. The three density functionals predict comparable IR intensities as shown in Table 2, but in the present investigation we have compared the calculated IR intensities from BP86/6-31G* with the experimental intensities. Thus, BP86 predicts reasonable IR intensities, comparable to experiment for many of the vibrations; while for a few vibrations, the calculated intensities deviate considerably from experiment. Although in Table 3 we have presented the calculated IR intensities for all the isotopes of TAB using BP86/6-31G* due to the unavailability of the IR intensities of various isotopes of TAB, comparison of the calculated and experimental intensities has not been possible.

***cis*-Azobenzene (CAB). Geometrical Structure.** Since a comparative study (*vide supra*) of different density functionals with various basis sets for TAB led to the conclusion that the nonlocal DFT method, BP86 with 6-31G* basis set, provides the best descriptions for CAB, only the results obtained from BP86/6-31G* are discussed below. All the data from other functional forms and basis sets are available on request. The available X-ray data[28] for CAB suggests that the molecule is severely distorted from planarity, it possesses only a 2-fold axis of symmetry with the phenyl rings rotated by ∼53.5° with respect to the N═N−C plane. Complete geometry optimization carried out using BP86/6-31G* adopted C_2 symmetry for CAB. The equilibrium structure and atom numbering of CAB is depicted in Figure 1. A comparative study of the calculated bond distances, bond angles, and dihedral angles of CAB using BP86/6-31G* and the experimentally optimized parameters are shown in Table 4. The calculated N═N bond distance is overestimated by 0.011 Å compared to the X-ray data, whereas C−N is underestimated by 0.012 Å. Average C−C bond length is also overestimated by 0.02 Å. The origin of these differences may be due to the crystal-packing forces. The C−N═N bond angle differs from X-ray values by 2°, and the C−C−N and C−C−C angles deviate by 0.8° and 0.6°, respectively. X-ray diffraction shows that the dihedral angle at the N═N double bond is 8°, and the phenyl ring is rotated by about 53.3° about the C−N bond relative to a planar N═N−C arrangement whereas theoretically calculated values for these are 12° and 47.4°, respectively. Thus, the optimized structural parameters obtained from the DFT method, BP86/6-31G*, for CAB are in reasonable agreement to the observed X-ray values.[28]

Fundamental Frequencies of CAB. Only a few vibrational spectral studies are available for CAB[35,36,50] with qualitative vibrational assignments. On the basis of C_2 symmetry, 66 fundamentals of CAB involve 34 A and 32 B type vibrations. All fundamental modes are both IR and Raman active. A and B type modes can be identified only when they are resolved through the depolarization ratio of Raman intensity, since A and B type modes are expected to be polarized and depolarized, respectively, in the Raman spectrum. Due to the unavailability of the depolarization ratio values for CAB, both A and B species are assigned to the same band wherever calculated frequencies lie very close to each other. The computed (unscaled) frequencies as well as PEDs of the various vibrational modes of CAB are shown in Table 5. The calculated frequencies and IR intensities for A and B vibrations for the isotopomers of CAB, *viz.* $(C_6H_5)_2N^{15}N$, $(C_6H_5{}^{15}N)_2$, and $(C_6D_5N)_2$, are shown in Table 6. The observed frequencies from IR spectra[35] for CAB and $^{14}N,^{15}N$−CAB are also given for comparison in Table 6. Apart from the $^{14}N,^{15}N$−CAB IR data,[35] no experimental data is available for other isotopes. Therefore, the discussions are confined mainly to the theoretically calculated isotopic shifts of $^{14}N,^{15}N$−CAB, in relation to the experimental values.

In CAB, it is observed that the vibrations ν_{1-5} and ν_{35-40} shift by 800 cm^{-1} upon deuteration of all the H atoms of the phenyl rings. This confirms our assignment of C−H stretch. These modes occur in the same frequency range as that of TAB. The atomic displacements for the 29 A vibrations of CAB (excluding highest frequency C−H stretching modes) are available as Supporting Information (Figure IS). The modes ν_6, ν_7, ν_{11}, ν_{16}, ν_{17}, ν_{40}, ν_{41}, ν_{44}, ν_{49}, and ν_{50} at 1600, 1583, 1356, 1078, 1023, 1596, 1577, 1349, 1077, and 1022 cm^{-1}, respectively, are assigned mainly to the C−C stretch from the PEDs as shown in Table 5. These modes have their counterpart in TAB with slightly shifted frequencies and are coupled to different vibrations. In CAB these modes are coupled to the C−H ip bend. These vibrations do not change in frequency

TABLE 4: Optimized Geometrical Parameters of *cis*-Azobenzene in Its Ground State, Obtained from the BP86/6-31G* Calculation

	BP86	expt
	6-31G*	X-ray[a]
	Bond Lengths (Å)	
$N^2═N^1$	1.264	1.253
$C^3−N^2$	1.437	1.449
$C^5−C^3$	1.411	1.385
$C^7−C^5$	1.400	1.377
$C^9−C^7$	1.405	1.389
$C^{11}−C^9$	1.406	1.374
$C^{13}−C^{11}$	1.400	1.378
$C^{13}−C^3$	1.413	1.410
$H^{15}−C^5$	1.095	0.93
$H^{17}−C^7$	1.095	0.93
$H^{19}−C^9$	1.095	0.93
$H^{21}−C^{11}$	1.095	0.93
$H^{23}−C^{13}$	1.094	0.93
	Bond Angles (deg)	
$C^3−N^2═N^1$	123.9	121.9
$C^5−C^3−N^2$	116.3	117.3
$C^{13}−C^3−N^2$	123.1	122.5
$C^3−C^5−C^7$	120.0	120.0
$C^3−C^{13}−C^{11}$	119.6	118.7
$C^5−C^7−C^9$	120.1	120.8
$C^5−C^3−C^{13}$	119.7	119.8
$C^{13}−C^{11}−C^9$	120.5	121.7
$C^{11}−C^9−C^7$	119.7	119.0
$H^{15}−C^5−C^3$	118.6	
$H^{15}−C^5−C^7$	121.3	
$H^{23}−C^{13}−C^3$	119.7	
$H^{23}−C^{13}−C^{11}$	120.5	
$H^{21}−C^{11}−C^{13}$	119.4	
$H^{21}−C^{11}−C^9$	120.0	
$H^{19}−C^9−C^{11}$	120.0	
$H^{19}−C^9−C^7$	120.1	
$H^{17}−C^7−C^9$	120.1	
$H^{17}−C^7−C^5$	119.7	
	Dihedral Angles (deg)	
$C^4−N^1═N^2−C^3$	12.0	8.0
$C^6−C^4−N^1═N^2$	47.4	53.3

[a] Reference 28.

TABLE 5: Calculated Frequencies (in cm^{-1}) and PEDs of *cis*-Azobenzene for the Normal Vibrations of A ($\nu_1-\nu_{34}$) and B ($\nu_{35}-\nu_{66}$) Symmetries, Obtained from BP86/6-31G*

mode	expt[a]	BP86/6-31G*	PED (%)[b]	mode	expt[a]	BP86/6-31G*	PED (%)[b]
ν_1		3135	99 υ(C−H)	ν_{35}		3135	99 υ(C−H)
ν_2		3129	99 υ(C−H)	ν_{36}		3129	99 υ(C−H)
ν_3		3121	99 υ(C−H)	ν_{37}		3121	99 υ(C−H)
ν_4		3110	99 υ(C−H)	ν_{38}		3110	99 υ(C−H)
ν_5		3102	99 υ(C−H)	ν_{39}		3101	99 υ(C−H)
ν_6		1600	65 υ(C−C), 24 δ(C−H)	ν_{40}		1596	67 υ(C−C), 25 δ(C−H)
ν_7	1585	1583	67 υ(C−C), 23 δ(C−H)	ν_{41}	1575	1577	67 υ(C−C), 25 δ(C−H)
ν_8	1511	1512	61 υ(N═N), 12 δ(C−H), 11 υ(C−C), 10 υ(C−N)	ν_{42}	1477	1475	66 δ(C−H), 28 υ(C−C)
				ν_{43}	1441	1442	58 δ(C−H), 37 υ(C−C)
ν_9		1468	59 δ(C−H), 24 υ(C−C)	ν_{44}		1349	85 υ(C−C), 14 δ(C−H)
ν_{10}	1451	1449	57 δ(C−H), 36 υ(C−C)	ν_{45}	1294	1298	83 δ(C−H), 11 υ(C−C)
ν_{11}		1356	87 υ(C−C), 12 δ(C−H)	ν_{46}	1178	1175	64 δ(C−H), 20 υ(C−C), 15 υ(C−N)
ν_{12}	1309	1302	85 δ(C−H)				
ν_{13}	1178	1176	70 δ(C−H), 23 υ(C−C)	ν_{47}	1152	1158	88 δ(C−H), 11 υ(C−C)
ν_{14}	1152	1158	89 δ(C−H), 11 υ(C−C)	ν_{48}		1136	51 υ(C−N), 22 δ(C−H), 19 υ(C−C)
ν_{15}		1111	51 υ(C−N), 20 υ(C−C), 18 δ(C−H)	ν_{49}	1067	1077	44 υ(C−C), 46 δ(C−H)
ν_{16}	1067	1078	47 υ(C−C), 46 δ(C−H)	ν_{50}	1023	1022	68 υ(C−C), 24 δ(C−H)
ν_{17}	1023	1023	68 υ(C−C), 23 δ(C−H)	ν_{51}	988	985	34 δ(C−C), 34 υ(C−C), 16 δ(C−H), 14 δ(C−N)
ν_{18}	988	984	35 δ(C−C), 34 υ(C−C), 15 δ(C−H), 14 δ(C−N)	ν_{52}	968	950	76 γ(C−H), 23 τ(C−C)
ν_{19}	968	950	76 γ(C−H), 22 τ(C−C)	ν_{53}	920	924	90 γ(C−H)
ν_{20}	920	924	91 γ(C−H)	ν_{54}		891	85 γ(C−H)
ν_{21}		887	95 γ(C−H)	ν_{55}	834	827	37 γ(C−H), 22 δ(N═N), 19 υ(C−N), 10 τ(C−N)
ν_{22}	807	818	99 γ(C−H)				
ν_{23}	756	759	59 γ(C−H), 12 δ(C−C), 10 υ(C−N)	ν_{56}	807	816	96 γ(C−H)
ν_{24}		741	37 γ(C−H), 15 δ(C−C), 17 υ(C−N)	ν_{57}	756	754	51 γ(C−H), 13 υ(C−N), 13 δ(C−C)
ν_{25}	688	680	58 γ(C−H), 37 τ(C−C)				
ν_{26}		609	30 δ(C−C), 18 δ(C−H), 15 δ(C−N), 10 τ(N═N)	ν_{58}	700	691	85 γ(C−H)
				ν_{59}	662	674	64 τ(C−C), 31 γ(C−H)
ν_{27}	596	583	36 τ(N═N), 20 τ(C−C), 17 τ(C−N), 12 δ(C−H)	ν_{60}		606	46 δ(C−C), 27 δ(C−H), 22 δ(C−N)
ν_{28}	541	529	40 δ(C−C), 34 τ(C−C), 27 δ(C−H)	ν_{61}	492	489	29 τ(C−C), 28 γ(C−H), 10 υ(C−N)
ν_{29}		411	32 τ(C−C), 30 γ(C−H), 13 τ(N═N)				
ν_{30}	403	399	51 τ(C−C), 34 γ(C−H)	ν_{62}	441	438	47 τ(C−C), 36 γ(C−H)
ν_{31}		265	24 τ(C−C), 23 γ(C−H), 18 γ(C−N), 14 τ(C−N)	ν_{63}		394	53 τ(C−C), 35 γ(C−H)
				ν_{64}		268	32 δ(C−N), 28 γ(C−N), 15 τ(C−N)
ν_{32}		168	51 τ(C−N), 26 τ(N═N), 10 γ(C−N)				
ν_{33}		66	42 γ(C−N), 26 τ(N═N)	ν_{65}		151	67 γ(C−N), 11 γ(C−H)
ν_{34}		47	67 τ(C−N), 11 δ(N═N)	ν_{66}		46	84 τ(C−N)

[a] Reference 35. [b] υ indicates stretch; δ, in-plane bend; γ, out-of-plane bend; τ, torsion.

upon ^{15}N substitution, and the shift in frequency due to deuteration is also not very prominent as seen in Table 6. The vibrational modes ν_7, ν_{16}, ν_{17}, ν_{41}, ν_{49}, and ν_{50} have been observed in IR spectra[35] and assigned qualitatively on the basis of the experimentally observed isotopic shift when one N atom of the azo group is substituted by ^{15}N. In particular, the modes ν_{16} and ν_{49} (observed at 1067 cm^{-1}) are assigned[35] to the C−N stretch and ν_{17} and ν_{50} (observed at 1023 cm^{-1}) to the C−H ip bend. Experimentally,[35] it has also been observed that these modes undergo almost no change in frequency on ^{15}N substitution of one of the N atoms, which is consistent with our results. Thus, on the basis of calculated isotopic shifts and the PEDs, we reassign these vibrations ν_{16}, ν_{17}, ν_{49}, and ν_{50} to the C−C stretch that is coupled to the C−H ip bend. Further, the ν_{41} (1575 cm^{-1}) mode experimentally assigned to the C−C stretch is consistent with our results. Computed IR intensities are also in agreement with the experimental results for ν_7, ν_{16}, ν_{17}, ν_{41}, and ν_{50}; however, for ν_{49}, strong intensity is predicted in contrast to the experiment.

The ν_8 mode at 1512 cm^{-1} is assigned to the N═N stretch both from our results and experimental data.[35] The PEDs (given in Table 5) show that the C−H ip bend and C−C and C−N stretches are coupled to the main azo stretch. Thus, the calculated value is very close to the experimental N═N stretch which appears at 1511 cm^{-1}. From IR spectra, it is observed that ν_8 appears with medium intensity and undergoes a shift of 25 cm^{-1} when one N of the azo group is substituted by ^{15}N, whereas computation leads to a strong IR band for the N═N stretch with an isotopic shift of 19 cm^{-1}. The main azo stretch for CAB appears at a higher frequency compared to that for TAB due to increased nonplanarity in CAB, leading to greater double bond character in N═N. The vibrational modes ν_9, ν_{10}, ν_{12-14}, ν_{42}, ν_{43}, ν_{45-47} at 1468, 1449, 1302, 1176, 1158, 1475, 1442, 1298, 1175, and 1158 cm^{-1}, respectively, are assigned mainly to the C−H ip bend. These modes change by 100−300 cm^{-1} in frequency upon deuterium substitution, depending on the contribution of the C−D ip bend in the respective modes. Only a few of the modes, *viz.* ν_{12}, ν_{14}, and ν_{47}, have their counterparts with similar frequencies and mode descriptions for TAB. Our assignment and calculated IR intensities are in agreement with the experimental[35] intensities and the qualitative description for the modes ν_{13}, ν_{14}, ν_{46}, and ν_{47}. Further, Kubler *et al.*[35] assigned ν_{10}, ν_{12}, ν_{42}, and ν_{43} modes to the C−C stretch. Hence, we have reassigned these vibrations to the C−H ip bend as shown by the shifts observed on deuteration. Experiment results in weak IR intensities for ν_{10}, ν_{12}, and ν_{43} and medium intensity for ν_{42}. Our calculated IR intensities agree well for ν_{12} and ν_{42} but deviate considerably for ν_{10} and ν_{43}. The modes ν_{15} and ν_{48} at 1111 and 1136 cm^{-1} correspond mainly to the C−N stretch. No IR counterpart of these vibrations has been observed. These modes are coupled to the C−C stretch and C−H ip bend. Both the C−N stretching modes, ν_{15} and ν_{48}, shift by 1 cm^{-1} upon ^{15}N substitution of one of the N atoms and by 32 and 36 cm^{-1} on deuteration, consistent with the PEDs given in Table 5. The C−N stretching modes in CAB have their counterparts at 1131 and 1228 cm^{-1} in TAB. This increase in frequency indicates greater bond strength for C−N in TAB as compared to CAB. The vibrations ν_{18}, ν_{26}, ν_{28}, ν_{51}, and ν_{60} at 984, 609, 529, 985, and 606 cm^{-1}, are assigned mainly to the C−C ip bend, all of which have their counterparts in the

TABLE 6: Calculated Frequencies (in cm^{-1}) for Isotopic Derivatives of *cis*-Azobenzene for the Normal Vibrations of A and B Symmetry, Obtained from BP86/6-31G*

		$(C_6H_5N)_2$			$(C_6H_5)_2N^{15}N$			$(C_6H_5{}^{15}N)_2$		$(C_6D_5N)_2$	
mode	character	expt[a]	calc	I[b]	expt[a]	calc	I[b]	calc	I[b]	calc	I[b]
					A Symmetry						
ν_1	υ(C−H)		3135	4.3		3135	4.3	3135	4.3	2323	4.6
ν_2	υ(C−H)		3129	0.8		3129	0.8	3129	0.8	2316	0.4
ν_3	υ(C−H)		3121	25.3		3121	25.2	3121	25.2	2307	13.8
ν_4	υ(C−H)		3110	1.9		3110	1.9	3110	1.9	2295	0.5
ν_5	υ(C−H)		3102	0.5		3102	0.5	3102	0.5	2285	0.4
ν_6	υ(C−C)		1600	2.0		1598	0.8	1597	0.3	1569	8.6
ν_7	υ(C−C)	1585 sh	1583	0.5	1585	1583	0.4	1583	0.3	1549	0.7
ν_8	υ(N═N)	1511 m	1512	55.4	1486	1493	51.3	1481	33.4	1501	43.3
ν_9	δ(C−H)		1468	0.1		1464	1.9	1454	5.3	1360	0.0
ν_{10}	δ(C−H)	1451 w	1449	3.7	1451	1448	5.5	1445	18.9	1337	1.1
ν_{11}	υ(C−C)		1356	0.0		1356	0.0	1356	0.0	1328	0.9
ν_{12}	δ(C−H)	1309 w	1302	0.1	1309	1302	0.1	1302	0.1	1023	0.0
ν_{13}	δ(C−H)	1178 w	1176	0.4	1178	1176	0.4	1176	0.4	944	0.5
ν_{14}	δ(C−H)	1152 w	1158	0.2	1152	1158	0.2	1158	0.2	862	0.4
ν_{15}	υ(C−N)		1111	0.0		1110	0.0	1109	0.0	1079	0.1
ν_{16}	υ(C−C)	1067 m	1078	1.0	1066	1078	1.0	1078	1.0	838	0.1
ν_{17}	υ(C−C)	1023 m	1023	1.4	1023	1023	1.4	1023	1.4	821	0.5
ν_{18}	δ(C−C)	988 w	984	0.2	988	984	0.2	984	0.2	813	0.6
ν_{19}	γ(C−H)	968 w	950	0.1	968	950	0.1	950	0.0	788	0.2
ν_{20}	γ(C−H)	920 s	924	0.3	917	924	0.5	924	0.3	753	1.1
ν_{21}	γ(C−H)		887	0.4		887	0.4	886	0.4	745	0.0
ν_{22}	γ(C−H)	807 w	818	1.6	807	818	1.6	818	1.6	705	3.3
ν_{23}	γ(C−H)	756 s	759	12.8	754	758	13.4	757	13.4	643	0.6
ν_{24}	γ(C−H)		741	0.7		739	0.5	736	0.3	635	0.3
ν_{25}	γ(C−H)	688 s	680	16.3	688	680	16.1	680	15.9	584	0.0
ν_{26}	δ(C−C)		609	0.1		608	0.0	608	0.0	558	0.1
ν_{27}	τ(N═N)	596 m	583	4.7	592	579	4.9	574	5.0	535	11.8
ν_{28}	δ(C−C)	541 w	529	0.1	538	527	0.1	524	0.1	485	3.6
ν_{29}	τ(C−C)		411	2.4		409	2.4	407	2.3	385	3.4
ν_{30}	τ(C−C)	403 w	399	0.0	403	399	0.0	398	0.0	350	0.2
ν_{31}	τ(C−C)		265	0.3		265	0.8	265	0.3	246	0.2
ν_{32}	τ(C−N)		168	0.2		167	0.2	167	0.2	158	0.2
ν_{33}	γ(C−N)		66	0.4		66	0.4	66	0.4	61	0.4
ν_{34}	τ(C−N)		47	0.0		47	0.0	47	0.0	44	0.0
					B Symmetry						
ν_{35}	υ(C−H)		3135	7.7		3135	7.7	3135	7.7	2323	13.4
ν_{36}	υ(C−H)		3129	54.4		3129	54.4	3129	54.4	2316	26.9
ν_{37}	υ(C−H)		3121	9.4		3121	9.4	3121	9.4	2307	2.9
ν_{38}	υ(C−H)		3110	15.7		3110	15.7	3110	15.7	2295	6.1
ν_{39}	υ(C−H)		3101	2.2		3101	2.2	3101	2.2	2285	1.2
ν_{40}	υ(C−C)		1596	1.3		1596	1.3	1596	1.3	1562	0.6
ν_{41}	υ(C−C)	1575 m	1577	4.0	1575	1577	4.0	1577	4.0	1540	1.9
ν_{42}	δ(C−H)	1477 m	1475	4.2	1477	1475	4.2	1475	4.2	1353	0.5
ν_{43}	δ(C−H)	1441 w	1442	6.4	1441	1442	6.4	1442	6.4	1346	0.7
ν_{44}	υ(C−C)		1349	2.4		1349	2.4	1349	2.4	1316	2.8
ν_{45}	δ(C−H)	1294 w	1298	1.7	1294	1298	1.7	1298	1.7	1024	0.2
ν_{46}	δ(C−H)	1178 w	1175	0.4	1178	1175	0.5	1175	0.5	945	0.5
ν_{47}	δ(C−H)	1152 w	1158	0.0	1152	1158	0.0	1158	0.0	865	0.3
ν_{48}	υ(C−N)		1136	3.9		1135	3.8	1133	3.7	1100	1.1
ν_{49}	υ(C−C)	1067 m	1077	11.4	1066	1076	11.3	1076	11.3	839	3.6
ν_{50}	υ(C−C)	1023 m	1022	3.0	1023	1022	3.0	1022	3.7	829	17.1
ν_{51}	δ(C−C)	988 w	985	1.6	988	985	1.6	984	1.6	823	0.3
ν_{52}	γ(C−H)	968 w	950	1.0	968	950	0.9	950	0.9	810	5.5
ν_{53}	γ(C−H)	920 s	924	0.4	917	924	0.5	924	0.5	775	0.2
ν_{54}	γ(C−H)		891	21.6		890	20.8	889	20.1	747	4.2
ν_{55}	γ(C−H)	834 w	827	4.2	834	821	2.5	818	0.4	724	9.9
ν_{56}	γ(C−H)	807 w	816	6.7	807	815	10.3	810	14.8	682	0.6
ν_{57}	γ(C−H)	756 s	754	38.0	754	752	39.4	750	40.6	636	3.0
ν_{58}	γ(C−H)	700 s	691	75.0	699	689	74.5	688	74.0	606	6.7
ν_{59}	τ(C−C)	662 sh	674	6.4	662	673	3.8	672	1.7	581	0.3
ν_{60}	δ(C−C)		606	0.1		606	0.1	606	0.1	533	48.8
ν_{61}	τ(C−C)	492 m	489	3.8	490	486	3.4	484	3.1	463	18.3
ν_{62}	τ(C−C)	441 m	438	6.5	439	437	6.5	435	6.5	399	1.5
ν_{63}	τ(C−C)		394	4.4		394	4.5	394	4.5	345	2.5
ν_{64}	δ(C−N)		268	6.6		266	5.9	264	6.2	257	6.6
ν_{65}	γ(C−N)		151	4.1		151	4.1	151	4.1	142	3.6
ν_{66}	τ(C−N)		46	1.5		46	1.5	46	1.5	43	1.3

[a] Reference 35. [b] I represents the infrared intensities in km/mol: sh, shoulder; m, medium; s, strong; w, weak.

spectra of TAB. From IR studies,[35] ν_{18} and ν_{51} (both observed at 988 cm^{-1} as weak bands) were assigned to the C−H oop bend, and ν_{28} (541 cm^{-1}, weak band) was described as a C−N ip bend. On the basis of our results, we have reassigned all three modes, ν_{18}, ν_{28}, and ν_{51}, to the C−C ip bend. Calculated IR intensities agree well with the experiment for ν_{18} and ν_{28},

but for ν_{51} medium intensity is predicted where as experiment reflects weak intensity.

It is observed from the PEDs in Table 5 that due to nonplanarity of the molecule, there is considerable mixing between the ip and oop vibrations, which is in sharp contrast to that observed in the case of TAB. The ν_{26} mode contains contributions from the C−H and C−N ip bends and the N═N torsion,[35] whereas for ν_{28}, the C−C torsion and C−H ip bend are coupled to the C−C ip bend. All the modes, ν_{18}, ν_{26}, ν_{28}, ν_{51}, and ν_{60} remain unchanged upon ^{15}N substitution and undergo a shift of ∼40−70 cm^{-1} on deuteration. The modes ν_{19-25} at 950, 924, 887, 818, 759, 741, and 680 cm^{-1} and ν_{52-58} at 950, 924, 891, 827, 816, 754, and 691 cm^{-1} are assigned to the C−H oop bend. Some of these modes are similar to those of TAB in frequency and mode description. Among these, ν_{19}, ν_{25}, and ν_{52} have contributions from C−C torsion. Experimentally,[35] ν_{22}, ν_{23}, and ν_{55-57} have been assigned to the C−H oop bend as observed in our calculations. ν_{23} and ν_{57} appear as strong IR bands both in experiment and calculation whereas ν_{22}, ν_{55}, and ν_{56} are observed to be weak from experiment. These modes are predicted to be of medium intensity from our calculations. ν_{20} and ν_{53} have been assigned to the C−N stretch, and ν_{25} and ν_{58} are reported to be C−C torsion by Kubler *et al.*[35] in contrast to our results. On the basis of the PED results, we reassign the modes ν_{20}, ν_{25}, ν_{53}, and ν_{58} to the C−H oop bend. All these bands appear with strong IR intensity in the experiment, but calculation predicts weak bands for ν_{20} and ν_{53} and intense peaks for ν_{25} and ν_{58}. The fundamentals ν_{23}, ν_{24}, ν_{55}, and ν_{57} have complex descriptions and consist of mixed ip and oop modes and have no counterpart in TAB. These modes undergo a shift of 100−150 cm^{-1} upon deuteration. The vibration ν_{27} with A symmetry corresponds to the N═N torsion coupled to the C−C, C−N torsion and C−H ip bend. This vibration shifts by about 4 cm^{-1} (consistent with experiment[35]) on isotopic substitution of one N atom of the azo group by ^{15}N, and it undergoes 9 cm^{-1} and 48 cm^{-1} shifts with complete substitution of the azo group by ^{15}N and deuterium as is shown in Table 6. The ν_{27} band appears with weak intensity both in experiment and calculation. The vibrational modes ν_{29-31}, ν_{59}, and ν_{61-63} at 411, 399, 265, 674, 489, 438, and 394 cm^{-1} have been assigned to C−C torsion. These modes are coupled to C−H oop modes and change little upon ^{15}N substitution but by 20−30 cm^{-1} on deuteration. ν_{61} (observed at 492 cm^{-1}) was assigned to C−N torsion which has been reassigned from our calculations to C−C torsion, as shown in table 5. The assignment[35] of the mode ν_{59} (662 cm^{-1}) is similar to our assignment. Only a few of these vibrations, ν_{29}, ν_{59}, ν_{61}, and ν_{63}, have their counterparts in TAB, which is shifted in frequency but is almost similar in description. ν_{30} and ν_{59} are observed to be weak in IR from experiment but are shown to be weak and of medium intensity from the calculation. ν_{61} and ν_{62} appear with medium intensity both from experiment and calculation. ν_{32}, ν_{34}, and ν_{66} modes at 168, 47, and 46 cm^{-1} are assigned to C−N torsion, and these vibrations hardly shift upon isotopic substitution of ^{15}N and D_{10}. The modes ν_{33} and ν_{65} at 66 and 151 cm^{-1} correspond to the C−N oop bend and are coupled to the N═N torsion and C−H oop bend. The ν_{64} mode at 268 cm^{-1} is assigned to the C−N ip bend that is coupled to the C−N oop bend and C−N torsion. This mode shifts by 2 and 4 cm^{-1} upon ^{15}N substitution of one and both N atoms of the azo group. It also shifts by 11 cm^{-1} due to complete deuteration of the phenyl rings. No experimental data is available for these low-frequency modes. All the low-frequency modes have no counterpart in the vibrational spectra of TAB. A comparison of the computed and the experimental frequencies from IR studies[35] shows an excellent agreement for CAB. The calculated RMS deviation for the computed (unscaled) frequencies of CAB (from BP86/6-31G*) is found to be 8 cm^{-1}.

Overall, the essential differences between the vibrational spectra of CAB and TAB can be summarized as follows. TAB is slightly distorted from planarity whereas CAB is completely nonplanar. Due to the nonplanarity in the structure of CAB, there is considerable mixing of the ip and oop modes. Moreover, in CAB, the π-electron density is localized on the central N═N bond as compared to greater π-conjugation in TAB, leading to increased double-bond character for N═N. As a result, the main azo stretch of CAB, ν(N═N) and τ(N═N) vibrations appear at a higher frequency as compared to TAB. CAB exhibits more single-bond character for the C−N bond, because of which the C−N stretch appears at lower wavenumbers for CAB relative to that for TAB. In addition, there is an increase in the number of C−H bending modes in CAB as compared to that in TAB.

Summary

A systematic study of the vibrational analysis of TAB and CAB using RHF and various DFT methods have been carried out. The RMS deviations for the unscaled frequencies obtained from various DFT methods giving the best structural parameters have been calculated. It is observed that the DFT method BP86/6-31G* is very useful in predicting vibrational frequencies for polyatomic systems like azobenzene. The frequencies, obtained from BP86/6-31G*, show a RMS deviation of 11 cm^{-1} for TAB and 8 cm^{-1} for CAB. These computed frequencies are in good agreement with the experimental frequencies for both isomers of azobenzene. Thus, we find that the performance of the DFT approach for polyatomic molecules is comparable to the widely used SQM approach for which the deviation of the computed frequencies is about 10 cm^{-1} of the experimental frequencies.[72,73] Further, we have clarified the asssignments for various vibrational modes of both isomers of azobenzene, TAB and CAB, from our calculations in addition to providing normal mode descriptions and IR intensities for all the normal vibrations, facilitating accurate vibrational assignments of experimental data. We have also pointed out the main differences in the vibrational spectra of TAB and CAB on the basis of the respective molecular structures.

Acknowledgment. We thank the Council of Scientific and Industrial Research and Department of Science and Technology, Government of India, for financial support. We also thank the Supercomputer Education and Research Centre, Indian Institute of Science, for providing us with the computing facilities necessary to carry out the present calculation.

Supporting Information Available: Tables of the optimized geometrical parameters, calculated frequencies and approximate mode vibrational assignments of TAB, and the figures of the normal mode pictures of the 29 A vibrations of CAB (19 pages). Ordering information is given on any current masthead page.

References and Notes

(1) Rau, H. *Photochromism. Molecules and Systems*; Durr, H., Bouas-Laurent, H., Eds.; Elsevier: Amsterdam, 1990; Chapter 4. p 165.

(2) (a) Bach, H.; Anderle, K.; Fuhrmann, Th.; Wendorff, J. H. *J. Phys. Chem.* **1996**, *100*, 4135. (b) Liu, Z.; Zhao, C.; Tang, M.; Cai, S. *J. Phys. Chem.* **1996**, *100*, 17337. (c) Taniike, K.; Matsumoto, T.; Sato, T.; Ozaki, Y.; Nakashima, K.; Iriyama, K. *J. Phys. Chem.* **1996**, *100*, 15508. (d) Barrett, C. J.; Natansohn, A. L.; Rachon, P. L. *J. Phys. Chem.* **1996**, *100*, 8836. (e) Schonhoff, M.; Mertesdorf, M.; Losche, M. *J. Phys. Chem.* **1996**, *100*, 7558. (f) Jaschke, M.; Schonherr, H.; Wolf, H.; Butt, H.-J.; Bamberg, E.; Besocke, M. K.; Ringsdorf, H. *J. Phys. Chem.* **1996**, *100*, 2290. (g) Xia, W. S.; Huang, C. H.; Ye, X. Z.; Luo, C. P.; Gan, L. B.; Liu, Z. F. *J. Phys. Chem.* **1996**, *100*, 2244.

(3) Ramanujam, P. S.; Hvilsted, S.; Andruzzi, F. *Appl. Phys. Lett.* **1993**, *62*, 1041.
(4) Lee, G. J.; Kim, D.; Lee, M. *Appl. Opt.* **1995**, *34*, 138.
(5) Ramanujam, P. S.; Hvilsted, S.; Zebger, I.; Siesler, H. W. *Macromol. Rapid Commun.* **1995**, *16*, 455.
(6) Hvilsted, S.; Andruzzi, F.; Ramanujam, P. S. *Opt. Lett*. **1992**, *17*, 1234.
(7) Willner, I.; Rubin, S. *Angew. Chem., Int. Ed. Engl.* **1996**, *35*, 367.
(8) Cimiraglia, R.; Hofmann, H-J. *Chem. Phys. Lett.* **1994**, *217*, 430.
(9) Rau, H.; Yu-Quan, S. *J. Photochem. Photobiol. A* **1988**, *42*, 321.
(10) Cimiraglia, R.; Asano, T.; Hofmann, H-J. *Gazz. Chim. Ital.* **1996**, *126*, 679.
(11) Hamm, P.; Ohline, S. M.; Zinth, W. *J. Chem. Phys.* **1997**, *106*, 519.
(12) Asano, T.; Cosstick, K.; Furuta, H.; Matsuo, K.; Sumi, H. *Bull. Chem. Soc. Jpn.* **1996**, *69*, 551.
(13) Sanchez, A. M.; de Rossi, R. H. *J. Org. Chem.* **1996**, *61*, 3446.
(14) Biswas, N.; Umapathy, S. *Chem. Phys. Lett.* **1995**, *234*, 24.
(15) Monti, S.; Orlandi, G.; Palmieri, P. *Chem. Phys.* **1982**, *71*, 87.
(16) Sension, R. J.; Repinec, S. T.; Szarka, A. Z.; Hochstrasser, R. M. *J. Chem. Phys.* **1993**, *98*, 6291.
(17) Myers, A. B.; Mathies, R. A. *J. Chem. Phys.* **1984**, *81*, 1152.
(18) Saltiel, J.; Sun, Y.-P. *Photochromism. Molecules and Systems*; Durr, H., Bouas-Laurent, H., Eds.; Elsevier: Amsterdam, 1990; p 64.
(19) Waldeck, D. H. *Chem. Rev.* **1991**, *91*, 415.
(20) (a) Saltiel, J.; D'Agostino, J.; Megarity, E. D.; Metts, L.; Neuberger, K. R.; Wrighton, M.; Zafiriou, O. C. *Organic Photochemistry*; Chapman, O. L., Ed.; Marcel Dekker: New York, 1973; Vol. 3, p 1. (b) Saltiel, J.; Charlton, J. L. *Rearrangements in Ground and Excited States*; de Mayo, P., Ed.; Academic Press: New York, 1980; Vol. 3, p 25.
(21) Majima, T.; Tojo, S.; Ishida, A.; Takamuku, S. *J. Phys. Chem.* **1996**, *100*, 13615 and references therein.
(22) Langkilde, F. W.; Wilbrandt, R.; Brouwer, A. M.; Negri, F.; Zerbetto, F.; Orlandi, G. *J. Phys. Chem*. **1994**, *98*, 2254 and references therein.
(23) Hartley, G. S.; Le Fevre, R. J. W. *J. Chem. Soc.* **1939**, 531.
(24) Bullock, D. J. W.; Cumper, C. W. N.; Vogel, A. I. *J. Chem. Soc.* **1965**, 5316.
(25) Kellerer, B.; Hacker, H. H.; Brandmuller, J. *Ind. J. Pure Appl. Phys.* **1971**, *9*, 903.
(26) Bouwstra, J. A.; Schouten, A.; Kroon, J. *Acta Crystallogr*. **1983**, *C39*, 1121.
(27) Traetteberg, M.; Hilmo, I.; Hagen, K. *J. Mol. Struct.* **1977**, *39*, 231.
(28) Mostad, A.; Romming, C. *Acta Chem. Scand.* **1971**, *25*, 3561.
(29) Rau, H.; Luddecke, E. *J. Am. Chem. Soc*. **1982**, *104*, 1616.
(30) Rau, H. *J. Photochem.* **1984**, *26*, 221.
(31) Sampiringue, N.; Guyot, G.; Monti, S.; Bortolus, P. *J. Photochem.* **1987**, *37*, 185.
(32) Lunak, S., Jr.; Nepras, M.; Hrdina, R.; Mustroph, H. *Chem. Phys.* **1994**, *184*, 255.
(33) Dyck, R. H.; McClure, D. S. *J. Chem. Phys.* **1962**, *36*, 2326.
(34) Lednev, I. K.; Ye, T.-Q.; Hester, R. E.; Moore, J. N. *J. Phys. Chem.* **1996**, *100*, 13338.
(35) Kubler, V. R.; Luttke, W.; Weckherlin, S. *Z. Elektrochem.* **1960**, *64*, 650.
(36) Le Fevre, R. J. W.; O'Dwyer, M. F.; Werner, R. L. *Aust. J. Chem.* **1953**, *6*, 341.
(37) Okamoto, H.; Hamaguchi, H.; Tasumi, M. *Chem. Phys. Lett.* **1986**, *130*, 185.
(38) Biancalana, A.; Campani, E.; Gorini, G.; Masetti, G.; Quaglia, M. *J. Raman Spectrosc*. **1992**, *23*, 155.
(39) Biancalana, A.; Campani, E.; Domenico, G. Di; Gorini, G.; Masetti, G.; Quaglia, M. *J. Raman Spectrosc.* **1993**, *24*, 43.
(40) Lorriaux, J. L.; Merlin, J. C.; Dupaix, A.; Thomas, E. W. *J. Raman Spectrosc.* **1979**, *8*, 81.
(41) Machida, K.; Lee, H.; Saito, Y.; Uno, T. *J. Raman Spectrosc*. **1978**, *7*, 184.
(42) Hacker, H. *Spectrochim. Acta* **1965**, *21*, 1989.
(43) Merlin, J. C.; Lorriaux, J. L.; Thomas, E. W.; Dupiax, A. *J. Raman Spectrosc.* **1981**, *11*, 209.
(44) Cataliotti, R. S.; Murgia, S. M.; Paliani, G.; Poletti, A.; Zgierski, M. Z. *J. Raman Spectrosc*. **1985**, *16*, 251.
(45) Cataliotti, R. S.; Murgia, S. M.; Paliani, G.; Poletti, A.; Zgierski, M. Z. *J. Raman Spectrosc.* **1985**, *16*, 258.
(46) Cataliotti, R. S.; Morresi, A.; Paliani, G.; Poletti, A.; Zgierski, M. Z. *J. Raman Spectrosc.* **1989**, *20*, 601.
(47) Barker, I. K.; Fawcett, V.; Long, D. A. *J. Raman Spectrosc.* **1987**, *18*, 71.
(48) Houben, J. L.; Masetti, G.; Campani, E.; Gorini, G. *J. Raman Spectrosc.* **1982**, *13*, 15.
(49) Curtis, R. D.; Hilborn, J. W.; Wu, G.; Lumsden, M. D.; Wasylishen, R. E.; Pincock, J. A. *J. Phys. Chem.* **1993**, *97*, 1856.
(50) Klima, M. I.; Kotov, A. V.; Gribov, L. A. *J. Struct. Chem*. **1972**, *13*, 987.
(51) Armstrong, D. R.; Clarkson, J.; Smith, W. E. *J. Phys. Chem*. **1995**, *99*, 17825.
(52) Stephens, P. J.; Devlin, F. J.; Chablowski, C. F.; Frisch, M. J. *J. Phys. Chem.* **1994**, *98*, 11623.
(53) (a) Handy, N. C.; Maslen, P. E.; Amos, R. D.; Andrews, J. S.; Murray, C. W.; Laming, G. J. *Chem. Phys. Lett*. **1992**, *197*, 506. (b) Handy, N. C.; Murray, C. W.; Amos, R. D. *J. Phys. Chem.* **1993**, *97*, 4392.
(54) El-Azhary, A. A.; Suter, H. U. *J. Phys. Chem.* **1995**, *99*, 12751.
(55) Boesch, S. E.; Wheeler, R. A. *J. Phys. Chem.* **1995**, *99*, 8125.
(56) Walden, S. E.; Wheeler, R. A. *J. Phys. Chem*. **1996**, *100*, 1530.
(57) Wong, M. W. *Chem. Phys. Lett.* **1996**, *256*, 391.
(58) Lee, S. Y.; Boo, B. H. *J. Phys. Chem.* **1996**, *100*, 8782.
(59) Lee, S. Y.; Boo, B. H. *J. Phys. Chem.* **1996**, *100*, 15073.
(60) Nonella, M.; Brandli, C. *J. Phys. Chem.* **1996**, *100*, 14549.
(61) Nonella, M.; Tavan, P. *Chem. Phys.* **1995**, *199*, 17.
(62) El-Azhary, A. A.; Suter, H. U. *J. Phys. Chem.* **1996**, *100*, 15056.
(63) Wheeless, C. J. M.; Zhou, X.; Liu, R. *J. Phys. Chem.* **1995**, *99*, 12488.
(64) Keszthelyi, T.; Wilbrandt, R.; Bally, T.; Roulin, J.-L. *J. Phys. Chem.* **1996**, *100*, 16850.
(65) Keszthelyi, T.; Wilbrandt, R.; Bally, T. *J. Phys. Chem.* **1996**, *100*, 16843.
(66) Walden, S. E.; Wheeler, R. A. *J. Phys. Chem.* **1996**, *100*, 1530.
(67) Kwiatkowski, J. S.; Leszczynski, J. *J. Phys. Chem.* **1996**, *100*, 941.
(68) Qin, Y.; Wheeler, R. A. *J. Phys. Chem.* **1996**, *100*, 10554.
(69) Hout, R. F., Jr.; Levi, B. A.; Hehre, W. J. *J. Comput. Chem.* **1982**, *3*, 234.
(70) Zhon, X.; Fogarasi, G.; Liu, R.; Pulay, P. *Spectrochim. Acta* **1993**, *49A*, 1499.
(71) Arenas, J. F.; Tocon, I. L.; Otero, J. C.; Marcos, J. I. *J. Phys. Chem.* **1995**, *99*, 11392.
(72) Kozlowski, P. M.; Jarzecki, A. A.; Pulay, P.; Li, X.-Y.; Zgierski, M. Z. *J. Phys. Chem.* **1996**, *100*, 13985.
(73) Hernandez, V.; Ramirez, F. J.; Casado, J.; Lopez Navarrete, J. T. *J. Phys. Chem.* **1996**, *100*, 2907.
(74) (a) Heller, E. J. *Acc. Chem. Res.* **1981**, *14*, 368. (b) Myers, A. B.; Mathies, R. A. *Biological Applications of Raman Spectroscopy*, Spiro, T. G., Ed.; Wiley: New York, 1987; Vol. 2, p 1. (c) Myers, A. B. *Laser Techniques in Chemistry*, Myers, A. B., Rizzo, T. R., Eds.; Wiley: New York, 1995; Vol. 23, p 325.
(75) Frisch, M. J.; Trucks, G. W.; Schlegel, H. B.; Gill, P. M. W.; Johnson, B. G.; Robb, M. A.; Cheeseman, J. R.; Keith, T.; Petersson, G. A.; Montgomery, J. A.; Raghavachari, K.; Al-Laham, M. A.; Zakrzewski, V. G.; Ortiz, J. V.; Foresman, J. B.; Cioslowsski, J.; Stefanov, B. B.; Nanayakkara, A.; Challacombe, M.; Peng, C. Y.; Ayala, P. Y.; Chen, W.; Wong, M. W.; Andres, J. L.; Replogle, E. S.; Gomperts, R.; Martin, R. L.; Fox, D. J.; Binkley, J. S.; Defrees, D. J.; Baker, J.; Stewart, J. P.; Head-Gordon, M.; Gonzalez, C.; Pople, J. A. *Gaussian 94*, Revision C.2; Gaussian, Inc.: Pittsburgh, PA, 1995.
(76) Becke, A. D. *J. Chem. Phys.* **1993**, *98*, 5648.
(77) Becke, A. D. *Phys. Rev. A* **1988**, *38*, 3098.
(78) Lee, C.; Yang, W.; Parr, R. G. *Phys. Rev. B* **1988**, *37*, 785.
(79) Perdew, J. P. *Phys. Rev. B* **1986**, *33*, 8822.
(80) Slater, J. C. The self-consistent field for molecules and solids. *Quantum theory of molecules and solids*; McGraw-Hill: New York, 1974; Vol. 4.
(81) Vosko, S. J.; Wilk, L.; Nusair, M. *Can. J. Phys*. **1980**, *58*, 1200.
(82) Schlegel, H. B. *J. Comput. Chem.* **1982**, *3*, 214.
(83) Sundius, T. *Molvib*; Calculation of Harmonic Force Fields and Vibrational Modes of Molecules. QCPE # QCMP 103, Version 6, 1991.